Synthesis and characterization of size-controlled vanadium dioxide nanocrystals in a fused silica matrix

R. Lopez[a], L. A. Boatner, and T. E. Haynes
Solid State Division, Oak Ridge National Laboratory, Oak Ridge, Tennessee 37831

L. C. Feldman[b] and R. F. Haglund, Jr.
Department of Physics and Astronomy, Vanderbilt University, Nashville, Tennessee 37235

Vanadium dioxide single-crystal precipitates with controlled particle sizes were produced in an amorphous, fused SiO_2 host by the stoichiometric coimplantation of vanadium and oxygen ions and subsequent thermal processing. The effects of the vanadium dioxide nanocrystal size, nanocrystal morphology, and particle/host interactions on the VO_2 semiconductor-to-metal phase transition were characterized. VO_2 nanoparticles embedded in amorphous SiO_2 exhibit a sharp phase transition with a hysteresis that is up to 50 °C in width—one of the largest values ever reported for this transition. The relative decrease in the optical transmission in the near-infrared region in going from the semiconducting to the metallic phase of VO_2 ranges from 20% to 35%. Both the hysteresis width and the transition temperature are correlated with the size of the precipitates. Doping the embedded VO_2 particles with ions such as titanium alters the characteristics of the phase transition, pointing the way to control the hysteresis behavior over a wide range of values and providing insight into the operative physical mechanisms. © *2002 American Institute of Physics.*
[DOI: 10.1063/1.1503391]

INTRODUCTION

Vanadium dioxide (VO_2) is one of a number of transition-metal oxides that undergo either an insulator-to-metal or semiconductor-to-metal transition (SMT) at a characteristic phase-transition temperature. Following the early observations of Morin[1] in 1959, the physical properties of VO_2 and other oxides of vanadium in the region of the phase transition have been extensively investigated. In particular, the semiconductor-to-metal phase transition temperature of VO_2 (around 67 °C) has made this material a convenient system for exploring the physical mechanisms responsible for the SMT. On cooling through the phase transition, VO_2 undergoes a first-order SMT from a high-temperature, metallic tetragonal rutile phase to a low-temperature monoclinic, semiconducting form. The crystalline phase change is of the shear type, with a small dilation (0.044%).[2] The electrical and optical properties of VO_2 undergo significant and abrupt changes across this structural phase transition. The high-temperature phase exhibits metallic properties and strongly attenuates the transmission of incident light at all frequencies;[3] the low-temperature phase is a narrow band gap semiconductor[4] (band gap=0.7 eV) with a relatively high transparency in the infrared spectral region. It is precisely this near-room-temperature transition and the associated large optical and electrical property changes that have also made VO_2 a candidate material for a wide variety of technological applications such as thermochromic coatings,[5] optical and holographic storage,[6,7] fiber-optical switching devices,[8] laser scanners,[9] missile training systems,[10] and ul-

trafast optical switching.[11] However, in order to incorporate the VO_2 properties into small-scale integrated optoelectronic devices, it is essential to fabricate and characterize VO_2 nanostructures including VO_2 nanocomposites. In this article, we describe practical methods for the preparation of VO_2 in the form of nanometer-size, single-crystal particles embedded in a fused SiO_2 host and characterize the properties of this finely divided form of VO_2.

In a previous brief letter,[12] we described the observation of VO_2 nanoprecipitates formed in amorphous SiO_2 by ion implantation. These nanoparticles exhibited a large hysteresis as compared to similar VO_2 precipitates formed in a (0001)-oriented single-crystal sapphire host.[13] It is commonly assumed in the VO_2 thin-film literature that, given a controlled oxide stoichiometry, the sharpness of the phase transition[14] as well as its hysteresis width and critical temperature are dependent on the stress[15] and microstructure of the films.[16] In the present work, the ability to control the size of the VO_2 precipitates allows us to effectively separate these effects and thereby develop a deeper understanding of the materials physics associated with the phase transition.

MATERIALS SYNTHESIS

High-purity fused silica substrates (Suprasil) were coimplanted at room temperature with vanadium and oxygen ions at various energies ranging between 100–300 and 36–120 keV for V and O, respectively. The implantation energies were calculated using the computer code TRIM[17] and were then selected to ensure the superposition of both the vanadium- and oxygen-implant distributions at the same depth in the near-surface region of the fused SiO_2 host. The formation of the VO_2 precipitates was achieved by a subse-

---

[a]Also at: Vanderbilt University. Electronic mail: rene.lopez@vanderbilt.edu
[b]Also at: Oak Ridge National Laboratory, Oak Ridge, TN 37831.
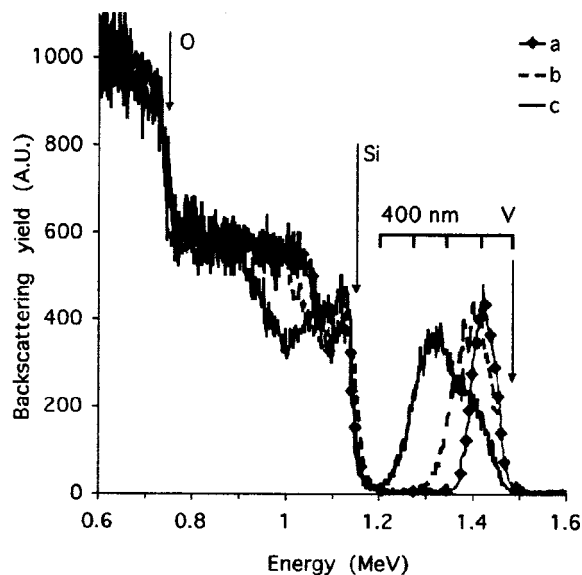
FIG. 1. Rutherford backscattering spectra for SiO_2 coimplanted with vanadium and oxygen in a 1:2 proportion are shown with the corresponding depth-matching energies. He^+ ions were incident with 2 MeV of initial energy and the backscattered particles were detected at a 160° angle. The indicated samples were annealed at 1000 °C in flowing argon in order to form VO_2 precipitates. (a) 1.0×10^{17} V ions/cm^2 at 100 keV, annealed 10 min, (b) 1.5×10^{17} V ions/cm^2 at 150 keV, annealed 60 min, and (c) 2.0×10^{17} V ions/cm^2 at 300 keV, annealed 90 min. The increasing ion straggling with increasing implantation energy produces progressively lower densities of the implanted ions for the same dose. The larger distance to the SiO_2 surface and the lower density increase the time required to achieve the desired VO_2 particle formation.

quent thermal annealing of the coimplanted specimens in flowing argon at atmospheric pressure and at temperatures ranging from 700 to 1000 °C for times of 2–60 min. In order to obtain a strong VO_2 response during the characterization procedures, the vanadium doses ranged from 1 to 2 $\times 10^{17}$ ions/cm^2 with oxygen implantation doses in the stoichiometric proportion for VO_2 formation. Rutherford backscattering spectrometry (RBS), as shown in Fig. 1, illustrates the distribution in-depth of the vanadium implants for different implant energies. It was observed that the volume density of implanted atoms tended to decrease with increasing implantation energy, due to the effects of straggling. Therefore, the optimal thermal annealing parameters for achieving controlled VO_2 precipitation would be different for each implant energy. Accordingly for purposes of consistency, the remainder of this article is restricted to samples that were implanted with vanadium and oxygen at 150 and 55 keV, respectively.

Vanadium, like most transition metals, can exist in different valence states and consequently, can form a variety of possible oxides (e.g., VO, V_2O_3, VO_2, and V_2O_5). In addition to these "simple" oxides, there are many other closely related structures where vanadium atoms have different valences between those of V_2O_3 and VO_2. The series V_nO_{2n-1} ($9 > n > 1$) between VO_2 and V_2O_3, as well as V_2O_5, V_4O_9, V_6O_{13}, and V_3O_7 have all been observed.[18] Therefore, it is not surprising that the phase equilibria in the vanadium-oxygen system[19] proved to be relatively complex. Accordingly, achieving a high degree of control over the oxygen partial pressure is indispensable for the formation of
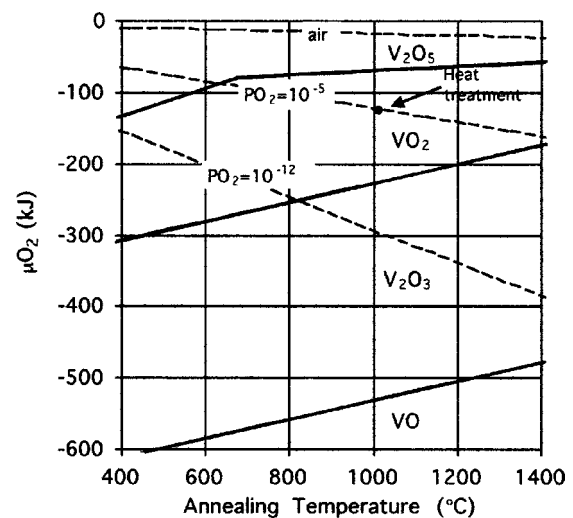

FIG. 2. The Ellingham diagram for the V–O system (excluding the complex oxides) shows the necessary, but not sufficient, external conditions (oxygen partial pressure and temperature) required to allow the reaction $V + O_2 \rightarrow VO_2$ to proceed in the forward direction.

a desired specific oxide of vanadium. In order to form VO_2, the present experiments were carried out in an atmosphere of flowing high-purity argon ($PO_2 \sim 10^{-5}$). The Ellingham diagram for the principal vanadium oxides[20] (as given in Fig. 2) shows that, at this partial pressure, a heat treatment above 625 °C is necessary for the formation of VO_2 to be thermodynamically allowed. (Experiments showed that nucleation and growth of nanoparticles occurred at 700, 800, 900, and 1000 °C, but not at 600 °C; the lower temperatures, naturally, resulted in longer annealing and growth times). Once the range of allowed processing temperatures for VO_2 formation was determined, subsequent experiments were carried out at a practical working temperature of 1000 °C, i.e., at a temperature that resulted in a fairly rapid precipitation and particle-formation process. These processing conditions are in fact necessary; from Fig. 2, it is clear that annealing in argon $+ 4\%$ H_2 ($PO_2 \sim 10^{-12}$), in air, or in pure oxygen will not result in VO_2 formation. However, these conditions do not necessarily guarantee VO_2 precipitation, since the reaction occurs inside the silica substrate. Silica proved to be an ideal host because, in addition to its well-known thermal stability, silicon does not dope VO_2 since the Si^{4+} ion is too small to occupy the VO_2 octahedral site.[21,22]

The additional condition that was determined to be necessary to ensure VO_2 formation was a minimum implanted oxygen dose. Figure 3 shows the final stoichiometry of the particles as a function of the implanted oxygen/vanadium ratio for samples implanted using both SiO_2 and Al_2O_3 hosts. A vanadium/oxygen ratio in SiO_2 less than 1:2 was determined by x-ray analysis to precipitate $VO_{1.84}$. When the implantation was carried out using Al_2O_3 as substrate, on the other hand, the material was more tolerant to oxygen deficiency. In both cases, adding extra oxygen usually produced a "blistering" of the host surface. Clearly, an appropriate internal oxygen concentration needs to be produced by the implanted oxygen atoms; moreover if the oxygen concentration is too high, the implanted oxygen atoms may diffuse in
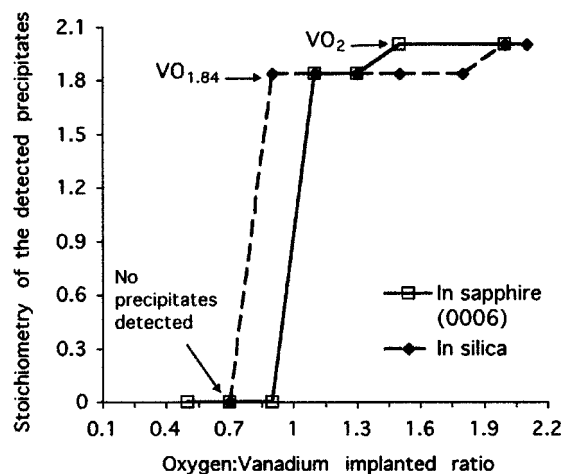
FIG. 3. Influence of implanted oxygen on the formation of vanadium oxide precipitates and their stoichiometry. All of the samples were implanted with 1.5×10^{17} V ions/cm^2 and annealed in high purity argon at 1000 °C for 30 min. In order to obtain vanadium oxide concentrations similar to those produced in SiO$_2$, the single-crystal sapphire samples were implanted with vanadium at 300 keV and with oxygen at 120 keV. Implants in SiO$_2$ were carried out at 150 and 55 keV, for V and O, respectively. The identification of the resulting oxide phases was performed using x-ray diffraction and by analyzing the infrared optical behavior.

FIG. 4. X-ray $\theta - 2\theta$ scans ($\lambda = 1.5406$ Å) of fused SiO$_2$ implanted with 2.0×10^{17} V ions/cm^2 at 150 keV and 4.0×10^{17} O ions/cm^2 at 55 keV and later annealed in flowing high-purity argon at 1000 °C for 30 min. The characteristic VO$_2$ diffraction lines detected at 27.81° and 57.67° correspond to the (011) and (022) monoclinic planes, respectively.

a manner leading to oxygen coalescence or "out-diffusion" rather than forming the metal oxide. Therefore, achieving proper control of the oxygen dose and its uniform distribution in the near-surface region in order to assure the necessary local stoichiometric ratio is essential for producing VO$_2$ precipitates inside SiO$_2$. Under the optimal conditions indicated by the arrow in the phase diagram in Fig. 2, optical, x ray, and other diagnostics showed no evidence for the formation in the SiO$_2$ host of oxides of vanadium other than VO$_2$.

In order to control the size of the precipitates, all other preparation conditions being the same, the annealing time was used to limit the particle growth. The annealing furnace was preheated to the desired temperature and then evacuated to a pressure of 5×10^{-6} Torr prior to introducing the high-purity argon and establishing a constant gas flow. The sample was remotely inserted into the high-temperature zone and was held in the hot zone for a controlled interval of time. The sample was then cooled to room temperature by a quick remote withdrawal (i.e., a withdrawal that maintained the established argon atmosphere until the sample had cooled to room temperature) from the furnace hot zone.

MATERIALS CHARACTERIZATION AND PERFORMANCE

The VO$_2$-particle/ SiO$_2$-host samples were characterized using RBS, x-ray diffraction (XRD), transmission electron microscopy (TEM), and infrared optical transmission techniques. As shown in Fig. 1, the RBS spectrum gives the depth distribution of the vanadium ions prior to the annealing and precipitate-formation step. The RBS spectrum also shows the absence of heavy impurities, no vanadium surface atoms, and the nearly complete V implantation-dose retention. After annealing, the RBS spectra showed no significant changes, indicating that the implanted ions remain in the
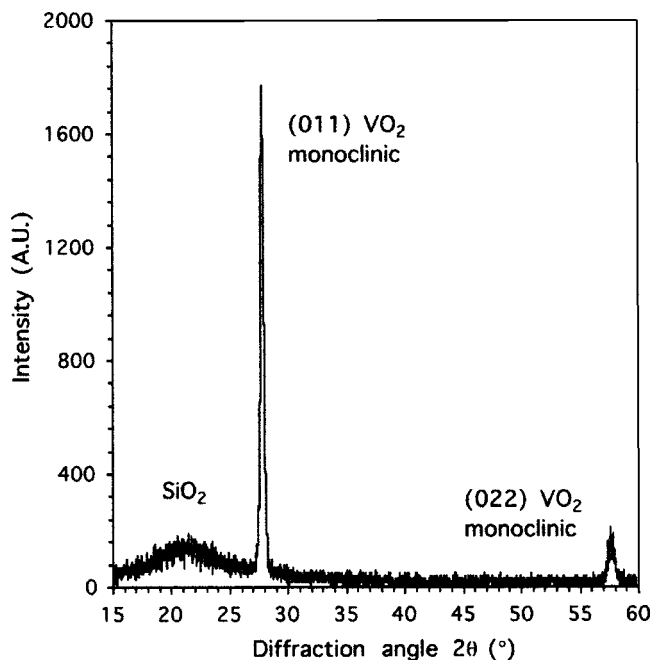
initial range distribution. The first confirmation that nanocrystalline VO$_2$ was formed by this process was provided by XRD, using standard $\theta - 2\theta$ scans at the Cu K_α wavelength and with the implanted surface lying perpendicular to the scattering vector. Figure 4 illustrates a typical room-temperature x-ray scan obtained after annealing the V- and O-implanted specimen at high temperature for 30 min. In addition to the broad structure due to the amorphous SiO$_2$ substrate, Bragg reflections at $2\theta = 27.81°$ and $57.67°$ were observed corresponding respectively to the (011) and (022) reflections of the VO$_2$ monoclinic phase. Since no other x-ray lines are observed, the VO$_2$ nanoparticles, in fact, are not only single crystalline, but also relatively highly oriented—in spite of the fact that the particles were formed in the amorphous fused silica host.

Figure 5 shows the equivalent d spacings for different annealing times ranging from 2 to 60 min. Also shown are various values of the (011) VO$_2$ monoclinic reflection as listed in different standard powder diffraction files (PDF). Although the relative intensity of the x-ray signal decreased somewhat for the shorter annealing times, the measured interatomic spacing in the nanoparticles remained relatively constant for all sizes.

The correlation of nanoparticle size with annealing time was directly established by TEM observations. All data are TEM bright-field images in which we employed mass contrast to identify the structures. Figure 6 shows a set of images taken at the same magnification on samples processed at various selected annealing times. It can be seen that the VO$_2$ particles initially precipitate in small spheroidal volumes and subsequently grow with increasing annealing time into bar-like shapes with an aspect ratio that is proportional to the
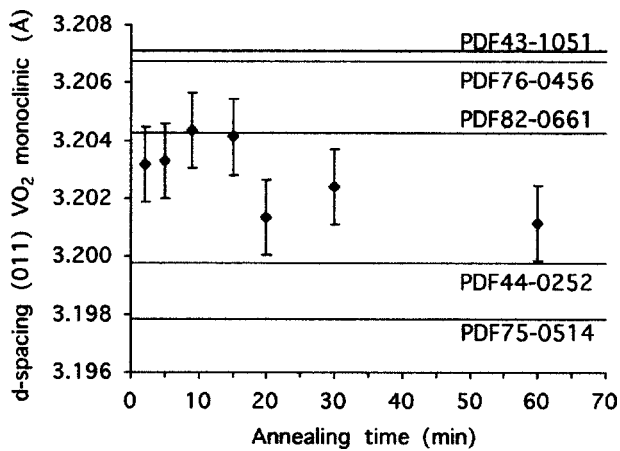
FIG. 5. Lattice spacings of the (001) VO$_2$ monoclinic planes as a function of the annealing time (in flowing high-purity argon at 1000 °C. The horizontal lines show the reference values obtained from several standard PDF. The SiO$_2$ substrates were implanted with 1.5×10^{17} V ions/cm^2 at 150 keV and 3.0×10^{17} O ions/cm^2 at 55 keV.

FIG. 7. (a) The TEM micrograph (200 keV, bright-field, mass contrast) shows that VO$_2$ precipitates exhibit some faceting even at the smaller particle sizes (annealed for 2 min.), (b) electron diffraction pattern obtained from a 100 nm long VO$_2$ particle, and (c) computer-generated electron diffraction pattern with the electron beam directed along the VO$_2$ monoclinic zone axis (011).

particle length. This growth in length takes place while the smallest particle dimension reaches a relatively constant value of ~80 nm. For the high-temperature (rutile) form of VO$_2$, the Bravais-Friedel law predicts a crystal shape that is determined by the {110} and {101} planes [the (110) tetragonal plane is the plane corresponding to the observed (011) monoclinic plane after the phase transition]. This geometric law that correlates the probability of a crystal form {hkl} with the interplanar spacing d_{hkl} has a simple physical basis given that the interaction energy between a growth layer and the
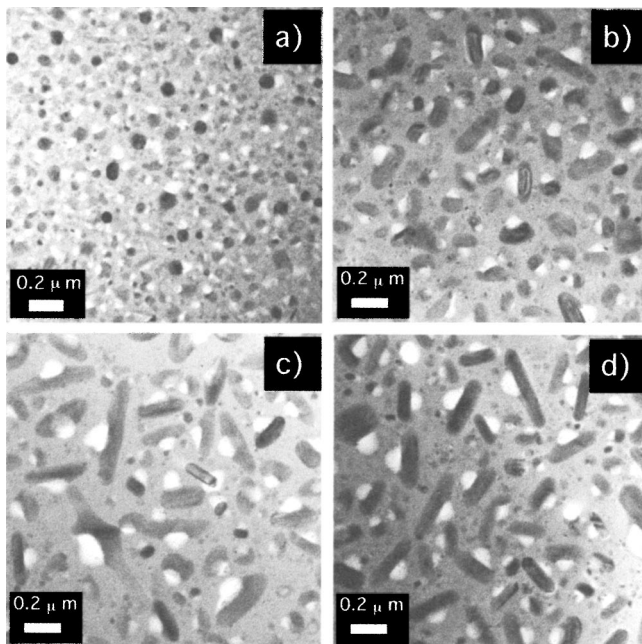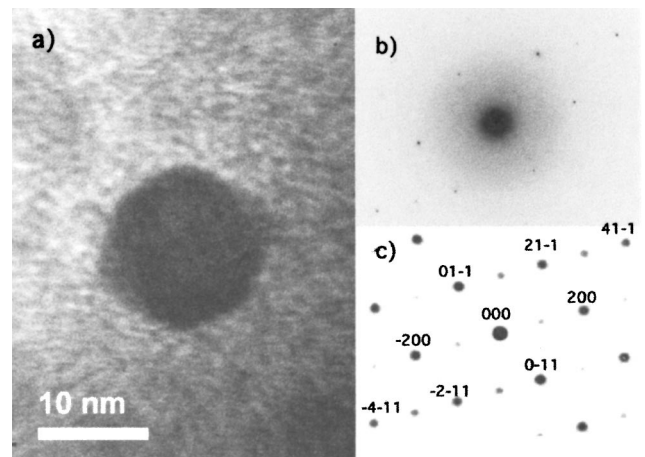
underlying crystal is generally smaller for large d_{hkl} values. In addition, if the growth rates are proportional to the attachment energies, simple ionic arguments indicate[23] that the elongated bar-like crystal habit grown on the {101} planes is, indeed, expected. This growth mechanism with preferential planes of attachment would explain the observed faceting in the early stages of the precipitate formation. The growth of VO$_2$ nanocrystals crystals with the *c* axis parallel to the surface corresponding to the texturing detected by x rays is an unexpected result whose origin is probably due to the ion implantation distribution and the growth mechanisms, however, presently it is not fully understood and remains to be investigated.

Figure 6 also shows the presence of nanovoids (white spots in the TEM micrographs) near a significant number of precipitates. These voids may be implicated in the initial particle nucleation process but this cannot be established definitively from the present results. Experiments employing *in situ* ion implantation and thermal processing in a TEM are planned in order to try to address both the issues of the texturing/orientation phenomena and the origin of the voids. Figure 7 shows a small faceted VO$_2$ nanocrystal along with the electron diffraction pattern displayed by these nanocrystals when they are properly aligned, that is, when the electron beam is parallel to a zone axis. The boundary planes for the faceted nanocrystals are likely to be {011} and {210} from the monoclinic structure.

In analyzing the characteristics of the VO$_2$ particles, the statistical distribution of the particle sizes has been calculated using the effective radius of the equivalent-volume sphere. Figure 8 shows the frequency distribution of the particles and the volume-weighted equivalent radius as a function of the annealing time. The broadening of the size distribution and the increasing mean size of the nanocrystals with increasing annealing times is typical of the formation of both metal and semiconductor nanocrystals by ion implantation and thermal annealing processes.

FIG. 6. Transmission electron microscopy images (200 keV, bright-field, mass contrast) of VO$_2$ precipitates formed at different annealing times: (a) 2, (b) 9, (c) 20, and (d) 60 min. Rapid precipitation and growth is observed during the first 30 min while longer annealing times did not result in significant additional growth. The samples were prepared by implanting SiO$_2$ with 1.5×10^{17} V ions/cm^2 at 150 keV and 3.0×10^{17} O ions/cm^2 at 55 keV and then annealing in argon at 1000 °C.
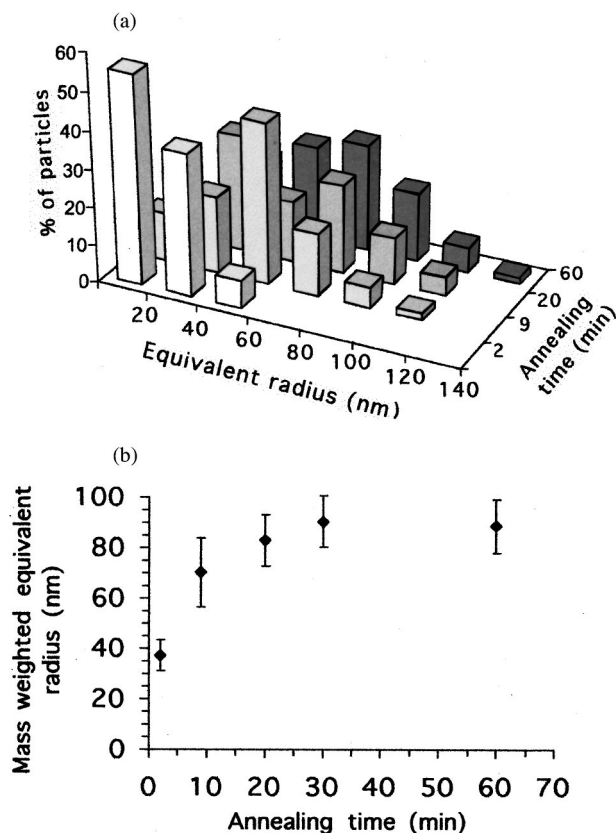
FIG. 8. (a) Size distribution of the precipitates as a function of the annealing time. (b) Mass-weighted mean equivalent radius.

A definitive confirmation of the formation of VO_2 is provided by the direct observation of the characteristic semiconductor-to-metal phase transition near 67 °C. Figure 9 shows the relative change in the optical transmission for selected mean crystal sizes. These measurements were carried out at normal incidence with 1.5 μm wavelength unpolarized
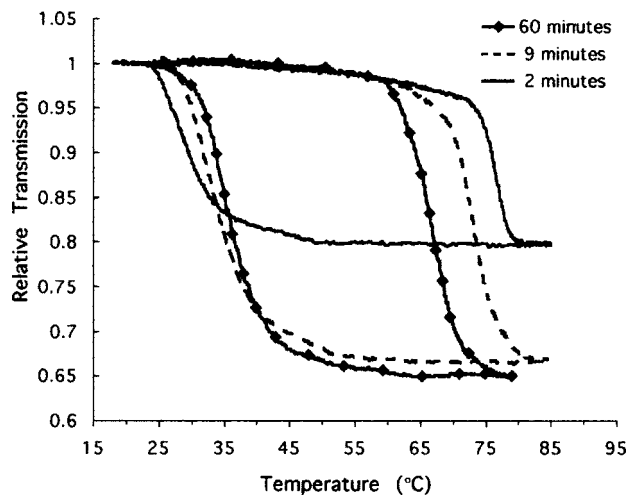

FIG. 9. Temperature dependence of the relative optical transmission at a wavelength of 1.5 μm for SiO_2 substrates implanted with 1.5 $\times 10^{17}$ V ions/cm² at 150 keV, 3.0 $\times 10^{17}$ O ions/cm² at 55 keV and annealed at 1000 °C for the indicated amount of time. The smallest VO_2 particles that are produced by the shortest annealing time exhibit the largest width in the hysteresis of the semiconductor-to-metal transition.

light from a HeNe laser while the temperature of the samples was ramped up and down at a rate of 2.5 °C/min using a Peltier thermoelectric device. The sample temperature was measured with a precision thermocouple in direct contact with the implanted side of the SiO_2 substrate.

Figure 9 shows that the annealing time and the corresponding size of the VO_2 precipitates exhibit a significant direct correlation with the transition temperatures and the width of the hysteresis curves. A reduction in the particle size increases the transition temperature when switching in the semiconductor-metal direction (i.e., on heating) from the standard value of 67 °C up to as high as $T = 76$ °C. On cooling, the transition temperature is also significantly reduced, generating an increasingly large hysteresis as the VO_2 crystals are reduced in size. In fact, the smallest precipitates exhibit hysteresis widths up to 50 °C, leaving the reverse (i.e., metal-to-semiconducting) transition temperature near room temperature.

We originally speculated that the large width of the VO_2 hysteresis in SiO_2, compared to that reported for VO_2 nanoparticles formed in (0001)-oriented sapphire,[24] may have its origin in the extrinsic stress created during the nanoparticle formation by the difference in thermal-expansion coefficients between the particles and the host matrix. However, experiments performed at lower annealing temperatures (700 °C) showed that this stress could not be primarily responsible for the observed energy barrier to the SMT. In fact, Fig. 5 suggests that neither the stoichiometry nor the stress experienced by the nanoparticles is affected by the relative duration of the annealing period—that is, by nanoparticle size.

The effect of the VO_2 stoichiometry on transition temperature has also been investigated.[25] Oxygen rich samples do not alter appreciably the transition temperature, and oxygen poor samples decrease the semiconductor-to-metal side of the hysteresis cycle by ~8°. Therefore, a nonstoichiometric oxygen fraction cannot explain the observed variation in the transition temperature.

Additional insight into the physics of the observed small-particle behavior is provided by the results of Ti doping experiments. Ti doping of the VO_2 precipitates is easily accomplished by implanting small quantities of titanium along with the vanadium and oxygen implant doses. Figure 10 shows a progressive increase of the metal-to-semiconductor transition temperature, and consequent narrowing of the hysteresis loop with the increasing concentration of Ti ions; there is also some steepening of the semiconductor-to-metal transition curve. Titanium forms a structure that is similar to that of tetragonal VO_2 and its addition has been reported to have little effect[26] on the SMT temperature in VO_2 bulk/thin films. These features point to structural defects as the source of the undercooling reduction in a manner that is analogous to the features that are observed in martensitic transformations.[27]

In fact, other structural defects could be responsible for the observed size effect, since they may play a role analogous to that played by nucleating defects in other solid-solid phase transitions.[28] In such models, although the density of those nucleating sites is independent of the size, the actual probability of finding a nucleation site must scale with clus-
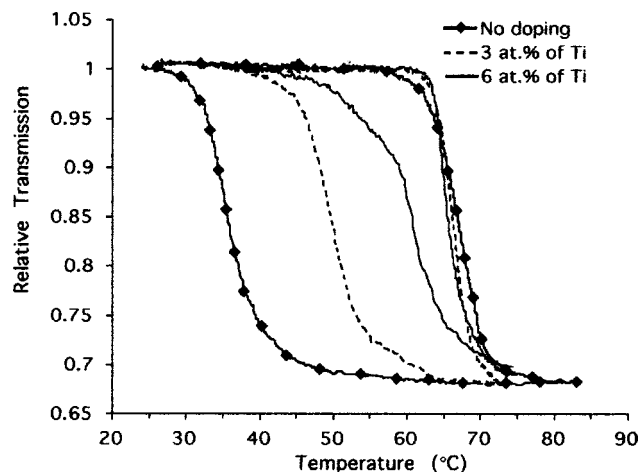
FIG. 10. Temperature dependence of the relative optical transmission at a wavelength of 1.5 μm of SiO_2 substrates implanted with 1.5×10^{17} V ions/cm^2 at 150 keV, the indicated Ti doping and the stoichiometric needed oxygen dose. Samples annealed at 1000 °C for 30 min.

ter volume. This would agree with our experimental observations, since we have noted that the transitions in the composites with smaller precipitates are thermally delayed and those particles need larger thermal driving forces to undergo the transition. Traditionally, deviations of the transition temperatures have been associated with the stress and microstructure of the samples. The observed increments in the transition temperatures for the smaller particles (following experimental pressure data[29] and the Clapeyron formula) would imply significant changes in the lattice constants and large hydrostatic pressures. However, given the results of Fig. 5, we can conclude this is not the case. In fact, there is no reason to suspect that the relative extent of the annealing period would change the strain of the precipitates given the high implantation doses employed in these experiments.[30] The observed correlation between the size and transition temperatures represents a true size effect and could in fact, through a heterogeneous nucleation model, clarify the early observations about the influence of the microstructure and grain size[16] in the phase transition of VO_2.

CONCLUSIONS

Size-controlled VO_2 precipitates have been formed in a fused silica host by the coimplantation of vanadium and oxygen ions in proper proportions and subsequent thermal annealing in a high-purity argon atmosphere at $T = 1000$ °C. The resulting VO_2 nanoprecipitates have hysteresis loops that are up to 50 °C wide and that exhibit a 20%–35% difference in the optical transmission between the semiconducting and metallic phases when measured in the near-infrared wavelength region. The precipitates grow with annealing time from small faceted spheroids into relatively larger bar-like shapes showing a clear preferential surface attachment of the constituent ions. A surprising degree of orientational order of the precipitates is observed even though the single-crystal particles are formed in an amorphous matrix. The transition temperatures show a direct correlation with the size of the nanocrystals. The extent of undercooling in the phase transition can be modified by Ti doping—thereby sug-

gesting a structural mechanism as the basis for the enhanced barrier to the "reverse" phase transition. The relative magnitude of the optical switching in the region of commonly used optical-communication wavelengths makes the near-surface nanocomposite system comprising VO_2 nanoparticles in a SiO_2 host of interest for the future development of applications in integrated optics geometries including fiber-optic and thin-film optical waveguides.

[1] F. J. Morin, Phys. Rev. Lett. **3**, 34 (1959).

[2] D. Kucharczyk and T. Niklewski, J. Appl. Crystallogr. **12**, 370 (1979).

[3] P. J. Hood and J. F. Natale, J. Appl. Phys. **70**, 376 (1991).

[4] B. Felde, W. Neissner, D. Schalch, A. Sharmann, and M. Werling, Thin Solid Films **305**, 61 (1997).

[5] C. G. Granqvist, Phys. Scr. **32**, 401 (1985).

[6] M. Fukuma, S. Zembutsu, and S. Miyazawa, Appl. Opt. **22**, 265 (1983).

[7] W. R. Roach, Appl. Phys. Lett. **19**, 453 (1971).

[8] C. E. Lee, R. A. Atkins, W. N. Giler, and H. F. Taylor, Appl. Opt. **28**, 4511 (1989).

[9] J. S. Chivian, W. E. Case, and D. H. Rester, IEEE J. Quantum Electron. **QE-15**, 1326 (1979).

[10] M. A. Richardson and J. A. Coath, Opt. Laser Technol. **30**, 137 (1998).

[11] M. F. Becker, A. B. Buckman, R. M. Wasler, T. Lepine, and P. Georges, Proc. SPIE **2189**, 400 (1994).

[12] R. Lopez, L. A. Boatner, L. C. Feldman, R. F. Haglund, Jr., and T. E. Haynes, Appl. Phys. Lett. **79**, 3161 (2001).

[13] L. A. Gea and L. A. Boatner, Appl. Phys. Lett. **68**, 3081 (1996).

[14] M. Borek, F. Quian, V. Nagabushnam, and R. K. Singh, Appl. Phys. Lett. **63**, 3288 (1993).

[15] F. Cardillo Case, J. Vac. Sci. Technol. A **2**, 1509 (1984).

[16] J. F. De Natale, P. J. Hood, and A. B. Harker, J. Appl. Phys. **66**, 5844 (1989).

[17] J. F. Ziegler, *Transport and Range of Ions in Matter, Ver. 96.01* (IBM Research, Yorktown Heights, NY, 1996).

[18] G. Nihuoul, Ch. Leroux, V. Madigou, and J. Durak, Solid State Ionics **117**, 105 (1999).

[19] J. S. Anderson and A. S. Kahn, J. Less-Common Met. **22**, 209 (1970).

[20] I. Yamaguchi, T. Manabe, T. Kumagai, W. Condo, and S. Mizuta, Thin Solid Films **366**, 294 (2000).

[21] J. B. MacChesney and H. J. Guggenheim, J. Phys. Chem. Solids **30**, 225 (1969).

[22] J. B. Goodenough, J. Solid State Chem. **3**, 490 (1971).

[23] *Crystal Growth: An Introduction*, edited by P. Hartman (North Holland, Amsterdam, 1973).

[24] L. A. Gea, J. D. Budai, and L. A. Boatner, J. Mater. Res. **14**, 2602 (1999).

[25] C. Blaauw, F. Leenhouts, F. van der Woude, and G. A. Sawatzky, J. Phys. C **8**, 459 (1975).

[26] F. Beteille, R. Morineau, J. Livage, and M. Nagano, Mater. Res. Bull. **32**, 1109 (1997).

[27] G. B. Staichowiak and P. G. McCormick, Acta Metall. **36**, 291 (1988).

[28] G. B. Olson and M. Cohen, *Dislocations in Solids* (Elsevier Science, Cambridge, MA, 1986), Vol. 7.

[29] C. N. Berglund and A. Jayarama, Phys. Rev. **185**, 1034 (1969).

[30] F. Harbsmeier, J. Conrad, and W. Bolse, Nucl. Instrum. Methods Phys. Res. B **136**, 505 (1998).